Prediction of a stable helium-hydrogen compound: First-principles simulations

Adebayo O. Adeniyi,[1] Adebayo A. Adeleke,[1] Xue Li,[2] Hanyu Liu,[2,3,*] and Yansun Yao[1,†]

[1]*Department of Physics and Engineering Physics, University of Saskatchewan, Saskatoon, Saskatchewan, Canada S7N 5E2*

[2]*International Center for Computational Method and Software and State Key Laboratory of Superhard Materials, College of Physics, Jilin University, Changchun 130012, China*

[3]*Key Laboratory of Physics and Technology for Advanced Batteries (Ministry of Education), International Center of Future Science, Jilin University, Changchun 130012, China*

(Received 4 December 2020; revised 17 May 2021; accepted 14 June 2021; published 2 July 2021)

Despite extensive experimental and theoretical work, consensus on the crystal structure and stability of the helium-hydrogen system is lacking. In this study, we investigate the possibility of helium forming a stable compound with hydrogen by using a first-principles structure search method. As a result of first-principles simulations, we predict a helium-hydrogen compound that is mechanically stable below 8 GPa with a $He(H_2)_3$ stoichiometry. Topological analysis of electron density at the bond critical points shows that there exists a quantifiable level of van der Waals interaction between helium and hydrogen in this $He(H_2)_3$ crystal. Our current results provide a case of weak interaction in a mixed hydrogen-helium system, offering insights for the evolution of interiors of giant planets such as Jupiter and Saturn.

DOI: 10.1103/PhysRevB.104.024101

I. INTRODUCTION

Among all the elements in the periodic table, helium is the most chemically nonreactive because of its complete outermost subshell with the highest ionization energy and almost zero electron affinity. At atmospheric conditions, helium is not known to form compounds with any other elements where there is actual negative energy of formation. Over the years, tremendous theoretical and experimental progress has been achieved in understanding the transformation of chemical bonding and formation of novel materials under extreme conditions of high pressure. Under high pressure, the electronic states of all atoms will change, which gives rise to novel compounds with unusual stoichiometry. Even chemically inert elements are found to become reactive at high pressures, particularly in rare gas solids made of noble gases such as the reaction of helium with alkali metals [1], ammonia [2,3], nitrogen [4], water [5,6], etc., under pressure.

Hydrogen and helium are the most abundant elements and ubiquitous in the universe; e.g., they contribute about 70%-95% to the mass of Saturn and Jupiter. One long unsettled question is why Saturn has about 50% more luminosity than predicted by existing models [7]. Both Saturn and Jupiter emit about twice the energy they receive from the Sun. A cooling model for homogeneous planets to estimate the luminosity of Jupiter produces a result that closely matches the measured value whereas the luminosity of Saturn is about 50% more than the model produces. This indicates that Saturn might have another source of energy that is much smaller or not present in Jupiter. One possible contribution to this additional energy in Saturn proposed is H-He demixing [8], in which heavier He droplets fall down from the H_2-He layer and exchange gravitational energy for thermal energy through viscous precipitation. The miscibility of H_2 in a He matrix or vice versa at high pressure plays an important role in deciding the phase diagrams of the H_2-He mixture. Theoretical studies have predicted the phase separation of H_2 and He at high pressures and temperatures [9], as well as the miscibility of H_2-He mixtures under planetary conditions [10]. The reactivity of He has also been demonstrated in helium hydrates, in which the He filled ice II and ice I_h were found to be energetically favorable against all decomposition reactions at 1 kbar [11]. In a recent experiment, spectral evidence showed that there can be sufficient mixing in a He-rich mixture for forming strong chemical association of H_2 to He at pressures below 100 GPa [12,13]. However, it was later argued that the Raman signal observed in the previous experiment was due to N_2 impurities and subsequent formation of N_2-H_2 van der Waals (vdW) solids at high pressure [14]. The question as to whether there is an interaction between helium and hydrogen that can lead to the formation of stable He-H compounds under the right conditions still remains unclear. To address the fundamental questions about the formation and evolution of these planetary bodies, there is a need to search for the relevant stable structures of H-He compounds.

In this paper, we therefore studied the helium-hydrogen-rich $[He\text{-}(H_2)_x]$ ($x = 1, 2, 3, 4, 5, 6$) systems using *ab initio* random structure search and first-principles calculations. We found a helium-hydrogen compound with a stoichiometry $He(H_2)_3$ and a negative formation enthalpy with respect to He and H_2 between 0 and 8 GPa. This $He(H_2)_3$ structure is shown to exhibit interaction between the H and He atoms that is similar to the vdW interaction found in He-O interactions for the helium filled ice II [15]. The $He(H_2)_3$ structure is also

*hanyuliu@jlu.edu.cn
†yansun.yao@usask.ca

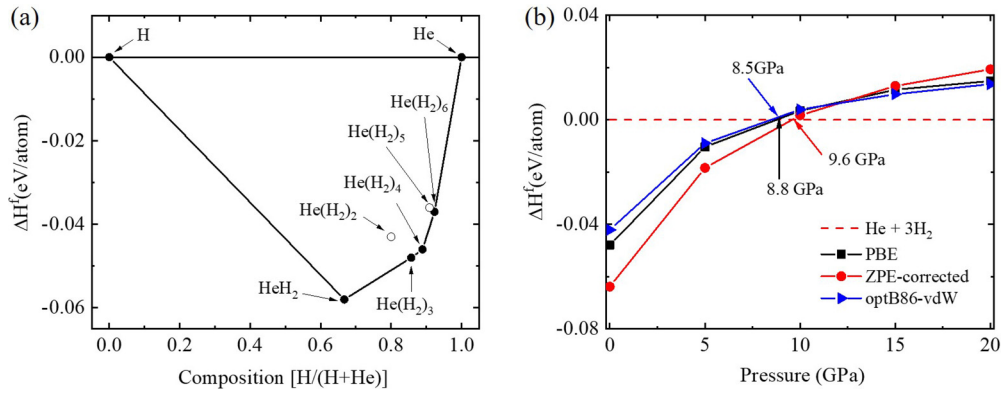

FIG. 1. (a) Calculated enthalpy of formation for all the considered He-H_2 compounds with respect to elemental decomposition at 0 GPa and 0 K. (b) Calculated enthalpy of formation for $He(H_2)_3$ with respect to He and $3H_2$. Black: PBE calculation without any energy correction; red: with inclusion of zero-point energy; blue: with inclusion of vdW interaction obtained from optB86-vdW functional.

found to be mechanically stable from the phonon calculations. The present results indicate the existence of a mixed helium-hydrogen system with an energetically favorable H-He interaction that may be sufficient for crystal solidification at low temperature and high pressure, enabling an understandable effect on the evolution of the interiors of gas giants.

II. METHODS

The structure search was performed with the *ab initio* random structure search method [16] at ambient pressure and zero temperature with primitive cells that contain one helium atom and two to 12 hydrogen atoms. We also performed structure searches for the He-H_2 system using the CALYPSO method [17] and found the same lowest energy structure of $He(H_2)_3$, validating the computational scheme in this study. Structural optimization, equation of states, electron localization function (ELF) [18], density of states (DOS), and electronic band structure were calculated using the Vienna *ab initio* simulation package (VASP) [19] with the projected augmented potentials (PAW) [20]. The H potential has the $1s^1$ valence state and He has the $1s^2$ valence state with the Perdew-Burke-Ernzerhof (PBE) exchange correlation functional [21]. The phonon dispersion relation of the structures was calculated with density functional perturbation theory [22] as implemented in VASP and postprocessed with the PHONOPY code [23]. The plane wave basis set was expanded with a kinetic energy cutoff of 800 eV and a dense k-point grid with spacing of 0.5 $Å^{-1}$. Topological analysis of the charge density was carried out with the quantum theory of atoms in molecules (AIM) [24] as implemented in the CRITIC2 code [25]. *Ab initio* molecular dynamics (AIMD) simulations were performed by employing an isothermal-isochoric (*NVT*) ensemble in a supercell with 448 atoms at 0 GPa using the VASP code. The AIMD trajectories were obtained from at least 10 ps long molecular dynamics (MD) simulations with Langevin dynamics sampled with a 0.5 fs time step. The equations of state for solid hydrogen, helium, and $He(H_2)_3$ were repeated using QUANTUM ESPRESSO [26] with tight norm-conserving PBE pseudopotentials generated using the OPIUM code [27], utilizing the cutoff radii of 0.80 and 0.77 Bohr for He and H, respectively. The kinetic energy cutoffs for wave functions and charge density used are 67 and 402 Ry, respectively.

III. RESULTS AND DISCUSSION

The search for the crystal structures of the He-H_2 system was performed at 0 GPa and 0 K. The convex hull of the He-H_2 system [Fig. 1(a)] constructed at 0 GPa indicates that several stoichiometries have negative enthalpy of formation with respect to the hexagonal close-packed (*hcp*) He and the hexagonal $P6_3/m$ phase of hydrogen. However, at atmospheric pressure (1 bar) the freezing point of hydrogen is extremely low (∼14 K) whereas helium does not solidify at all—it requires a pressure above 25 bars to solidify at zero temperature [28]. Therefore, the convex hull at 0 GPa does not necessarily suggest the formation of any He-H_2 compound since the enthalpy is not a sufficient measure of thermodynamic stability at ambient pressure. The formation of He-H_2 compounds is expected to occur at high pressures, where all phases solidify and the enthalpy becomes a meaningful factor of thermodynamic stability. For all He-H_2 compounds on the convex hull, $He(H_2)_3$ is the only dynamically and mechanically stable candidate (see phonon discussion later). For this reason, this work and the following discussion are focused on the $He(H_2)_3$ compound. To account for the solidification threshold of helium, the equation of state was estimated in a large pressure region from ambient pressure up to 20 GPa (0.2 Mbar) [Fig. 1(b)]. The predicted compound belongs to the triclinic P-1 space group and its formation is continuously favored at high pressures as established by the variation of ΔH^f with pressure in Fig. 1(b). Because of the light masses of hydrogen and helium, zero-point motion may have a large effect on the stability of the He-H system. Furthermore, at low temperatures, the fluctuation of electron distribution likely induces vdW interaction which is particularly notable for helium and hydrogen [29]. Thus, ΔH^f was corrected by adding zero-point energy (ZPE) contributions estimated using harmonic approximation, and vdW contribution obtained by using the optP86-vdW functional [30] (see Fig. 1). The calculation has been repeated using optPBE-vdW [31], optP88-vdW [31], and vdW-D2 [32] functionals, and semiempirical DFT-D3 method [33] (see Supplemental

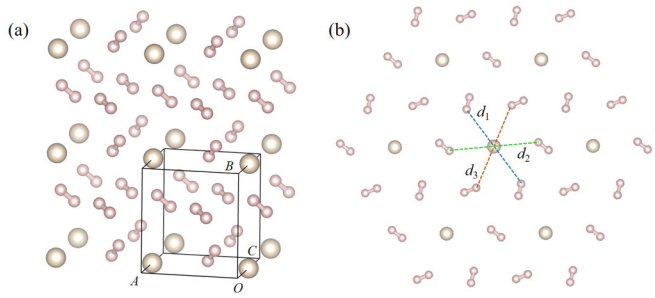

FIG. 2. (a) Crystal structure of $He(H_2)_3$ compound at ambient pressure. The unit cell is a slightly distorted cubic cell. (b) A single layer of $He(H_2)_3$ with three distinct He $\cdots$ H distances noted.

Material [34]). The result of the inclusion of ZPE increases the pressure for decomposition of $He(H_2)_3$ (to He and H_2 solids) from 8.8 to 9.6 GPa as seen in Fig. 1(b) while the application of the optP86-vdW functional slightly lowers the decomposition pressure to about 8.5 GPa. The inclusion of zero-point motion and vdW interaction supports the stability of the $He(H_2)_3$ solid under moderate pressures. To cross check the results, the ΔH^f were recalculated using QUANTUM ESPRESSO [26] with tight norm-conserving pseudopotential [35]. The results indicate a slight shift of decomposition pressure by $\sim$0.3 GPa, confirming the validity of the present results (see Fig. S2 in the Supplemental Material [34]). Although the current calculation shows that the $He(H_2)_3$ solid is more stable than its constituent He and H_2 solids at high pressure, we note that the standard DFT method may not sufficiently capture all factors contributing to the thermodynamic stability of light elements. The phonon calculation establishes that $He(H_2)_3$ is mechanically stable (see later), but an accurate determination of the thermodynamic stability of this solid requires a more sophisticated calculation method, to take nuclear quantum effects into consideration.

The crystal structure of $He(H_2)_3$ are shown in Fig. 2(a). The optimized structural parameters are presented in the Supplemental Material [34]. In this structure, the hydrogen atoms retain a diatomic form similar to that in solid hydrogen. The H_2 units are arranged in hexagonal layers similar to those in the solid hydrogen phase III [36] with helium atoms occupying the vertices [Fig. 2(b)]. On each layer there exist three different He-H distances and they are measured to be 2.604, 2.708, and 2.650 Å for d_1, d_2, and d_3, respectively. At the upper bound pressure of 8 GPa, these distances are reduced to 2.191, 2.212, and 2.198 Å. These He-H distances are within the sum of the vdW radii of helium (1.4 Å) and hydrogen (1.2 Å), suggesting that the presence of helium is paramount to the formation of the compound. The role of helium in the $He(H_2)_3$ solid is seen from a computational experiment at 0 GPa: After the removal of helium at 0 GPa, the structure becomes a *R*-3 lattice of hydrogen which immediately becomes unstable as evident from the large-magnitude imaginary frequencies in the phonon dispersion curve (Fig. S3 [34]). Thus, the role of helium is to stabilize the crystal; it is more than a physical spacer.

The results of the phonon dispersion calculation of the $He(H_2)_3$ crystal at 0 GPa [Fig. 3(a)] and at 8 GPa [Fig. 3(b)] show that the structure is dynamically stable and (in principle) experimentally accessible in this pressure range. The phonon calculation shows that all other He-H_2 compounds on the convex hull are unstable (Figs. S7–S9 [34]) and therefore are eliminated from consideration. At high pressure, the interaction between H_2 units and He is increased, as seen from the increase of the bandwidths in both the helium (low frequency) and hydrogen (high frequency) regions. Dynamical properties of the predicted $He(H_2)_3$ compound are examined by performing AIMD simulations at 0 GPa and temperature of 10, 50, and 100 K (see Supplemental Material [34]). We calculated the mean squared displacement [see Figs. S4(a), S4(d), S4(g)] and analyze the atomic motions in the trajectories [see Figs. S4(b), S4(c), S4(e), S4(f), S4(h), S4(i)]. The observation is that atoms oscillate around the equilibrium positions up to at least 10 K in the $He(H_2)_3$ compound, indicative of a solid [see Figs. S4(a) and S4(b)]. At 50 K, the motion of both the hydrogen and helium atoms become very large, evolving toward a amorphous or liquidlike phase [see Figs. S4(d) and S4(e)] while the system is seen as a liquid at 100 K [Figs. S4(g) and S4(h)]. These preliminary results suggest that if the $He(H_2)_3$ compound was to be stabilized at ambient pressure, its stable region should be very narrow near 0 K, but the region of stability is expected to increase with the pressure. It should also be noted that both hydrogen and helium contain significant nuclear quantum effects, and that molecular dynamics, even with incorporation of the path integral, cannot account

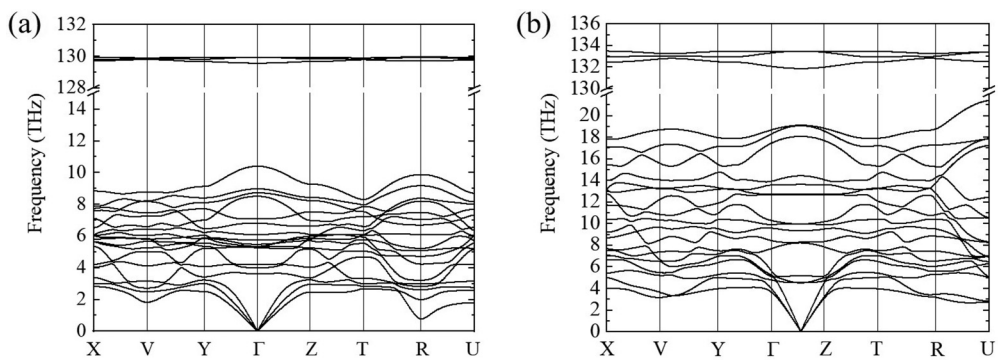

FIG. 3. Calculated phonon dispersion curves for the $He(H_2)_3$ compound (a) at 0 GPa and 0 K, and (b) at 8 GPa and 0 K. An axis break is added to the *y* axis to increase the visible region of the curves.

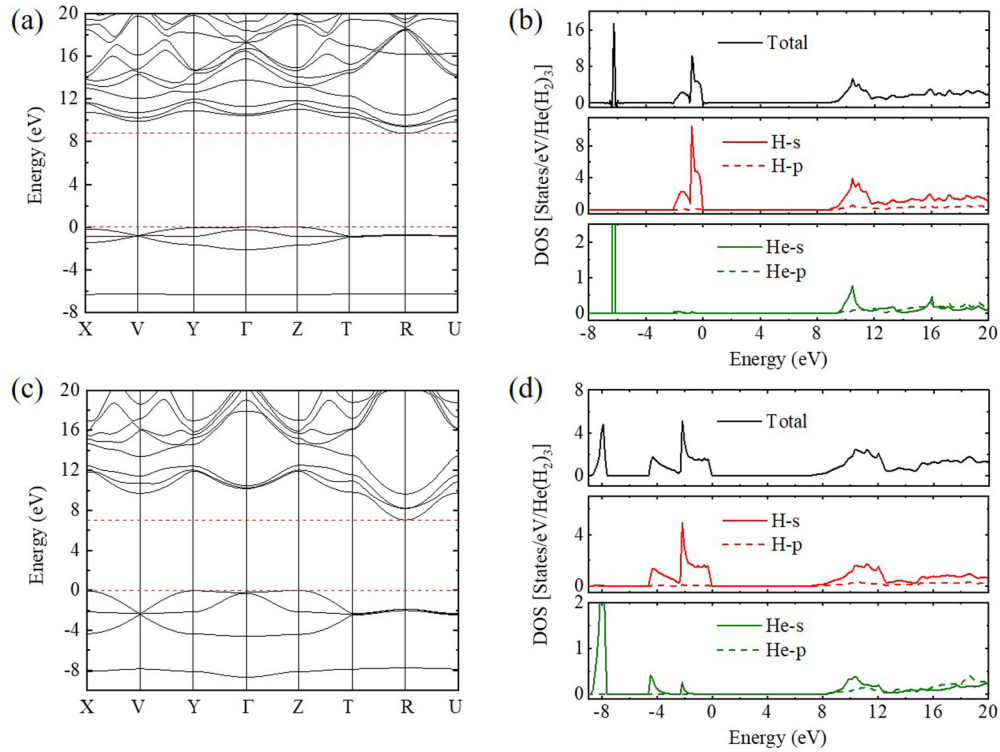

FIG. 4. (a) Electronic band structure and (b) projected DOS for the $He(H_2)_3$ compound at 0 GPa. (c) Electronic band structure and (d) projected DOS for the $He(H_2)_3$ compound at 8 GPa.

accurately for the dynamics of the system below 10 K [37]. The AIMD results here are only indicative, representing an upper bound estimation.

The calculated electronic band structure and projected DOS of $He(H_2)_3$ at ambient pressure and at 8 GPa [Figs. 4(a)–4(d)] reveal that this structure is a wide band gap insulator. At 0 GPa it possesses an indirect band gap of 8.49 eV which reduces to 7.04 eV at 8 GPa. The electronic DOS at ambient pressure shows that in the valence region, the hydrogen bands and helium band are well separated, indicative of very weak interaction. At higher pressure, the widths of all bands increase as a result of the enhanced interatomic interaction in the solid. This reveals that the intermolecular interaction within the H_2 units increases as a direct effect of compression, and the interaction between hydrogen and helium is enhanced also as seen from the slight orbital overlap from -5 eV to the Fermi level [Fig. 4(d)]. To understand the interaction between He and H, we have calculated the ELF, which is an indicative tool in the identification of places in a crystal structure where localization of electrons can be found. The result of the ELF calculation in the $He(H_2)_3$ crystal (see Supplemental Material [34]) shows that the hydrogen atoms in the H_2 units are covalently bonded as their electron clouds completely overlap. Moreover, the result shows that there are no electron accumulations between hydrogen and helium atoms, indicating that any interaction between He and H in this structure should be closed shell in nature, consistent with vdW interactions.

Topological analysis of charge density at the bond critical point (BCP) was done by using quantum theory of atoms in molecules (AIM) [24]. At 0 GPa, topological analysis identifies BCPs between the helium atom and each of the distinct hydrogen atoms in the structure. At ambient pressure, the calculated charge density $\rho(r_{BCP})$ at the BCP for d_1, d_2, and d_3 contacts [see Fig. 2(b)] are 0.019, 0.016, and 0.017 e^- Å^{-3}, respectively. These $\rho(r_{BCP})$ values are much lower than the expected values for conventional hydrogen bonds at ambient pressure (0.04–0.24 e^- Å^{-3}) [38,39], indicating much weaker He-H interaction. The calculated Laplacian $\nabla^2\rho(r_{BCP})$ for these BCPs are all positive, i.e., 0.266, 0.207, and 0.243 e^- Å^{-5}, respectively, which are consistent with the closed shell nature of the electron distribution. All other calculated properties at these three BCPs at 0 GPa are presented in Table S2 [34]. In addition, a complete table of all other BCPs (Table S6) in the structure at 0 GPa can be found in the Supplemental Material [34]. The results are consistent with weak vdW interactions similar to those found in He-O closed shell interactions for the helium filled ice II [5]. At 8 GPa, the calculated $\rho(r_{BCP})$ at BCPs for d_1, d_2, and d_3 contacts are 0.051, 0.049, and 0.050 e^- Å^{-3}, respectively, which are enhanced from the ambient pressure values driven by compression and approaching the low bound of the charge density for hydrogen bonding at ambient pressure. The respective $\nabla^2\rho(r_{BCP})$ are 0.783, 0.746, and 0.755 e^- Å^{-5}, also increased from the ambient values. Table S3 [34] shows all the calculated parameters at these three BCPs between helium and hydrogen at 8 GPa. A complete table of all other BCPs in the structure at 8 GPa is shown in Table S7 [34]. To put these results in perspective, we performed the same analysis on the pure elemental structures at 0 and 8 GPa. In the $P6_3/m$ hydrogen solid, at 0 GPa, noncovalent H-H contacts have $\rho(r_{BCP})$ that range from 0.029 to 0.035 e^- Å^{-3} with corresponding

$\nabla^2\rho(r_{BCP})$ from 0.365 to 0.436 e^- Å^{-5} as shown in Table S8 [34] whereas at 8 GPa, $\rho(r_{BCP})$ for the same contacts are from 0.069 to 0.077 e^- Å^{-3} with corresponding $\nabla^2\rho(r_{BCP})$ having values from 0.647 to 0.857 e^- Å^{-5} (see Table S9 [34]). For hcp helium, the He-He contacts have $\rho(r_{BCP})$ of 0.044 e^- Å^{-3} and $\nabla^2\rho(r_{BCP})$ of 1.109 e^- at 0 GPa, while at 8 GPa, $\rho(r_{BCP})$ increases to 0.061 e^- Å^{-3} with corresponding $\nabla^2\rho(r_{BCP})$ of 1.439 e^- Å^{-5}. Thus, it appears that the He-H interaction in $He(H_2)_3$ crystal is closed shell in nature, with the strength weaker than the vdW interaction along the He-He interaction in solid helium at the same pressure. Although these results are reported as obtained, it is important to point out that future work is required to completely understand all the properties and the stabilization mechanism of this $He(H_2)_3$ compound. In particular, the high pressure field has in recent years seen the emergence of atypical new compounds from chemical reactions that do not result in the formation of local chemical bonds [40]. Future theoretical and experimental analysis on the $He(H_2)_3$ compound could give significant insight into the rapidly increasing classes of compounds formed under pressure without an actual chemical bond [41].

It is worth noting that although the $He(H_2)_3$ compound is calculated to have lower enthalpy than the combination of constituent elements throughout the pressure range of consideration, the contribution of pressure-volume work to the enthalpy of the system prefers the decomposition of the compound at the aforementioned pressure (see Fig. S6 in the Supplemental Material [34]). In addition, despite the increasing interaction in the compound with pressure, which is evident with the reduction in interatomic distances, and supported by the comparison of the internal energy, the pressure-work contribution to the enthalpy grows faster in the compound than in the constituent elements and becomes significant enough to induce decomposition. It also should be emphasized that the temperature region for solidification is expected to be very narrow above 0 K. Due to the limit of theory, the freezing point of $He(H_2)_3$ at low pressures cannot be accurately calculated yet. The light masses of He and H mean an accurate calculation requires a full treatment of quantum effects; e.g., the quantum simulations include nuclear exchange at low temperature, while this kind of simulation is technically challenging and beyond the scope of this study. Phonon calculation establishes the dynamic stability of $He(H_2)_3$ at 0 K, indicating that this compound is accessible at very low temperatures. External compression will likely extend the stability of the compound to higher temperature regions.

IV. CONCLUSION

In summary, we predict a helium-hydrogen compound that is calculated to be dynamically stable at low pressures. This compound has $He(H_2)_3$ stoichiometry with an arrangement of atoms that showcases the importance of the presence of helium to the formation and stability of the structure. The phonon dispersion curve reveals dynamical stability of the structure at ambient conditions as well as a higher pressure of 8 GPa. Topological analysis of electron density at the bond critical points shows there exists weak vdW interaction between helium and hydrogen in the $He(H_2)_3$ crystal. This predicted compound contributes to our understanding of helium reactivity and H_2-He mixtures under planetary conditions.

ACKNOWLEDGMENTS

The authors express gratitude to the Information and Communications Technology group and the High-Performance Computing Training and Research Facilities at the University of Saskatchewan for providing access to the Plato cluster computing resource as well as the computing clusters of West Grid and Compute Canada. This project has the support of Natural Sciences and Engineering Research Council of Canada (NSERC).

[1] X. Dong, A. R. Oganov, A. F. Goncharov, E. Stavrou, S. Lobanov, G. Saleh, G.-R. Qian, Q. Zhu, C. Gatti, V. L. Deringer, R. Dronskowski, X.-F. Zhou, V. B. Prakapenka, Z. Konôpková, I. A. Popov, A. I. Boldyrev, and H.-T. Wang, Nat. Chem. **9**, 440 (2017).

[2] Y. Bai, Z. Liu, J. Botana, D. Yan, H.-Q. Lin, J. Sun, C. J. Pickard, R. J. Need, and M.-S. Miao, Commun. Chem. **2**, 102 (2019).

[3] J. Shi, W. Cui, J. Hao, M. Xu, X. Wang, and Y. Li, Nat. Commun. **11**, 3164 (2020).

[4] W. L. Vos, L. W. Finger, R. J. Hemley, J. Z. Hu, H.-K. Mao, and J. A. Schouten, Nature **358**, 46 (1992).

[5] H. Liu, Y. Yao, and D. D. Klug, Phys. Rev. B **91**, 014102 (2015).

[6] C. Liu, H. Gao, Y. Wang, R. J. Needs, C. J. Pickard, J. Sun, H.-T. Wang, and D. Xing, Nat. Phys. **15**, 1065 (2019).

[7] W. B. Hubbard, T. Guillot, M. S. Marley, A. Burrows, J. I. Lunine, and D. S. Saumon, Planet. Space Sci. **47**, 1175 (1999).

[8] J. J. Fortney, Science **305**, 1414 (2004).

[9] M. A. Morales, S. Hamel, K. Caspersen, and E. Schwegler, Phys. Rev. B **87**, 174105 (2013).

[10] M. Schöttler and R. Redmer, Phys. Rev. Lett. **120**, 115703 (2018).

[11] P. Teeratchanan and A. Hermann, J. Chem. Phys. **143**, 154507 (2015).

[12] J. Lim and C.-S. Yoo, Phys. Rev. Lett. **120**, 165301 (2018).

[13] J. Lim, M. Kim, S. Duwal, S. Kawaguchi, Y. Ohishi, H.-P. Liermann, R. Hrubiak, J. S. Tse, and C.-S. Yoo, Phys. Rev. B **101**, 224103 (2020).

[14] R. Turnbull, M.-E. Donnelly, M. Wang, M. Peña-Alvarez, C. Ji, P. Dalladay-Simpson, H.-k. Mao, E. Gregoryanz, and R. T. Howie, Phys. Rev. Lett. **121**, 195702 (2018).

[15] D. Londono, J. L. Finney, and W. F. Kuhs, J. Chem. Phys. **97**, 547 (1992).

[16] C. J. Pickard and R. J. Needs, Phys. Rev. Lett. **97**, 045504 (2006).

[17] Y. Wang, J. Lv, L. Zhu, and Y. Ma, Phys. Rev. B **82**, 094116 (2010).
[18] A. D. Becke and K. E. Edgecombe, J. Chem Phys. **92**, 5397 (1990).
[19] G. Kresse and J. Hafner, Phys. Rev. B **47**, 558 (1993).
[20] G. Kresse and D. Joubert, Phys. Rev. B **59**, 1758 (1999).
[21] J. P. Perdew, K. Burke, and M. Ernzerhof, Phys. Rev. Lett. **77**, 3865 (1996).
[22] S. Baroni, S. de Gironcoli, A. Dal Corso, and P. Giannozzi, Rev. Mod. Phys. **73**, 515 (2001).
[23] A. Togo, F. Oba, and I. Tanaka, Phys. Rev. B **78**, 134106 (2008).
[24] R. F. W. Bader, Chem. Rev. **91**, 893 (1991).
[25] A. Otero-de-la-Roza, E. R. Johnson, and V. Luaña, Comput. Phys. Commun. **185**, 1007 (2014).
[26] P. Giannozzi, S. Baroni, N. Bonini, M. Calandra, R. Car, C. Cavazzoni, D. Ceresoli, G. L. Chiarotti, M. Cococcioni, I. Dabo, A. Dal Corso, S. de Gironcoli, S. Fabris, G. Fratesi, R. Gebauer, U. Gerstmann, C. Gougoussis, A. Kokalj, M. Lazzeri, L. Martin-Samos, N. Marzari, F. Mauri, R. Mazzarello, S. Paolini, A. Pasquarello, L. Paulatto, C. Sbraccia, S. Scandolo, G. Sclauzero, A. P Seitsonen, A. Smogunov, P. Umari, and R. M. Wentzcovitch, J. Phys.: Condens. Matter **21**, 395502 (2009).
[27] OPIUM: The optimized pseudopotential interface unification module, http://opium.sourceforge.net/.
[28] J. M. McMahon, M. A. Morales, C. Pierleoni, and D. M. Ceperley, Rev. Mod. Phys. **84**, 1607 (2012).
[29] H. Margenau, Rev. Mod. Phys. **11**, 1 (1939).
[30] J. Klimeš, D. R. Bowler, and A. Michaelides, Phys. Rev. B **83**, 195131 (2011).
[31] J. Klimeš, D. R. Bowler, and A. Michaelides, J. Phys.: Condens. Matter **22**, 022201 (2010).
[32] K. Lee, É. D. Murray, L. Kong, B. I. Lundqvist, and D. C. Langreth, Phys. Rev. B **82**, 081101(R) (2010).
[33] S. Grimme, J Anthony, S. Ehrlich, and S. Krieg, J. Chem. Phys. **132**, 154104 (2010).
[34] See Supplemental Material at http://link.aps.org/supplemental/10.1103/PhysRevB.104.024101 for structure parameters, formation enthalpy, phonon dispersion relations, dynamical behaviors, electron localization functions, and topological analysis of candidate structures.
[35] N. Troullier and J. L. Martins, Phys. Rev. B **43**, 1993 (1991).
[36] C. J. Pickard and R. J. Need, Nat. Phys. **3**, 473 (2007).
[37] T. E. Markland and M. Ceriotti, Nat. Rev. Chem. **2**, 0109 (2018).
[38] U. Koch and P. L. A. Popelier, J. Phys. Chem. **99**, 9747 (1995).
[39] P. L. A. Popelier, J. Phys. Chem. A **102**, 1873 (1998).
[40] M. Miao, Y. Sun, E. Zurek, and H. Lin, Nat. Rev. Chem. **4**, 508 (2020).
[41] Z. Liu, J. Botana, A. Hermann, S. Valdez, E. Zurek, D. Yang, H.-q. Lin, and M.-s. Miao, Nat. Commun. **9**, 951 (2018).